Experimental and first-principles calculation study of the pressure-induced transitions to a metastable phase in GaPO4 and in the solid solution AlPO4-GaPO4

E. Angot, B. Huang, Claire Levelut, Rozenn Le Parc, Patrick Hermet, A. S. Pereira, G. Aquilanti, G. Frapper, Olivier Cambon, J. Haines

Experimental and first-principles calculation study of the pressure-induced transitions to a metastable phase in $GaPO_4$ and in the solid solution $AlPO_4$-$GaPO_4$

E. Angot,[1,2] B. Huang,[3] C. Levelut,[2] R. Le Parc,[2] P. Hermet,[1] A. S. Pereira,[4] G. Aquilanti,[5,*] G. Frapper,[3] O. Cambon,[1] and J. Haines[1,†]

[1]*ICGM, CNRS, Université de Montpellier, ENSCM, Montpellier, France*

[2]*L2C, CNRS, Université de Montpellier, Montpellier, France*

[3]*IC2MP UMR 7285, Université de Poitiers - CNRS, Poitiers, France*

[4]*Instituto de Física and Escola de Engenharia, Universidade Federal do Rio Grande do Sul, 91501-970 Porto Alegre, Rio Grande do Sul, Brazil*

[5]*European Synchrotron Radiation Facility (ESRF), 38343 Grenoble, France*

(Received 29 March 2017; revised manuscript received 10 July 2017; published 15 August 2017)

α-Quartz-type gallium phosphate and representative compositions in the $AlPO_4$-$GaPO_4$ solid solution were studied by x-ray powder diffraction and absorption spectroscopy, Raman scattering, and by first-principles calculations up to pressures of close to 30 GPa. A phase transition to a metastable orthorhombic high-pressure phase along with some of the stable orthorhombic *Cmcm* $CrVO_4$-type material is found to occur beginning at 9 GPa at 320 °C in $GaPO_4$. In the case of the $AlPO_4$-$GaPO_4$ solid solution at room temperature, only the metastable orthorhombic phase was obtained above 10 GPa. The possible crystal structures of the high-pressure forms of $GaPO_4$ were predicted from first-principles calculations and the evolutionary algorithm USPEX. A predicted orthorhombic structure with a $Pmn2_1$ space group with the gallium in sixfold and phosphorus in fourfold coordination was found to be in the best agreement with the combined experimental data from x-ray diffraction and absorption and Raman spectroscopy. This method is found to very powerful to better understand competition between different phase transition pathways at high pressure.

DOI: 10.1103/PhysRevMaterials.1.033607

I. INTRODUCTION

The discovery of the pressure-induced amorphization of α-quartz at pressures above 15 GPa [1] generated a great deal of interest in the origin of this phenomenon, which has been the subject of numerous experimental and theoretical studies. Amorphous material has also been reported to be present in addition to high-pressure crystalline phases [2], which highlights the competition between transitions to crystalline and amorphous forms [3] and the different transition pathways available at high pressure, many involving metastable states. α-Quartz homeotypes (GeO_2, BeF_2, PON, ABO_4: A = B, Al, Ga, Fe; B = P, As) provide models for the high-pressure behavior of silica and are also potential new materials with improved properties (e.g., piezoelectrics) [4]. Starting from the α-quartz- or α-berlinite-type structure (space group $P3_121$, $Z = 3$) for AO_2 or ABO_4 compounds, respectively, transitions to amorphous and/or crystalline phases have been reported for various α-quartz homeotypes [4,5]. In the case of $FePO_4$ [6], for example, simultaneous transitions to a $CrVO_4$ structure and an amorphous form were observed at 2.5 GPa. This $CrVO_4$ structure with mixed 6:4 cation coordination is also the stable high-pressure form for $AlPO_4$ and $GaPO_4$ [4–8]; however, thermal activation is often necessary in order to obtain this form [7,8]. The $CrVO_4$-type form is also obtained at room temperature from α-cristobalite-type $GaPO_4$ [9]; however, the behavior at ambient temperature starting with the α-berlinite-type form is less clear with the materials obtained at high pressure not always being well crystallized [10–13]. Several solid solutions exist between α-quartz homeotypes. In the case of the $AlPO_4$-$GaPO_4$, an x-ray diffraction study indicated that there is complete static Al/Ga disorder, which may open the way to design materials with tunable piezoelectric properties [14–16]. Up to the present, it is not known what influence preexistent static disorder has on the competition between transitions to crystalline or amorphous high-pressure phases. Our preliminary high-pressure data obtained by laboratory x-ray diffraction indicate, in addition to the presence of a $CrVO_4$-type phase, the formation of a new, unidentified, poorly crystallized phase in the Ga-rich region of the $AlPO_4$-$GaPO_4$ solid solution [17]. The combined use of x-ray absorption spectroscopy (XAS) and x-ray diffraction (XRD) as a function of pressure and temperature along with Raman scattering and first-principles calculations in the present study has enabled us to better understand the competition between this new phase and other crystalline or amorphous forms.

II. EXPERIMENTAL

A. Sample preparation

$GaPO_4$ powder was prepared by dissolving 4N gallium metal in nitric acid followed by precipitation with phosphoric acid. The powdered sample was washed, dried, and heated at 700 °C for 2 h in order to eliminate the maximum amount of hydroxyl groups. $Al_{0.30}Ga_{0.70}PO_4$ powder was synthesized by hydrothermal methods as described previously [15]. Solutions of $AlPO_4$ and $GaPO_4$ in sulfuric acid were mixed and placed in a PTFE-lined autoclave and heated in order to induce crystallization of $Al_{0.3}Ga_{0.7}PO_4$. The resulting powder was ground, passed through a 20 μm sieve, and annealed at 500 °C.

*Present address: Elettra Sincrotrone Trieste, s.s. 14, km 163.5, 34149 Basovizza, Trieste, Italy.

†julien.haines@umontpellier.fr

B. High-pressure XRD and XAS

$GaPO_4$ and $Al_{0.3}Ga_{0.7}PO_4$ were studied as a function of pressure and temperature of up to 32 GPa and 330 °C by XAS and XRD on the beamline ID24 at the ESRF [18]. High-pressure and high-pressure/high-temperature, energy-dispersive XAS measurements were performed at the Ga *K* edge (10.447 keV) and data were obtained up to 400 eV above the white line. XRD patterns were obtained using a wavelength of 1.202 Å and a Mar Research 345 imaging plate at a distance of 782 mm and offset from the direct beam to cover an angular range of 14°–32° in 2θ. The sample to detector distance was calibrated using a lanthanum hexaboride standard. The diffraction patterns were analyzed using the program FIT2D [19]. The samples were loaded in 90 to 120 μm holes in rhenium gaskets for the different runs in a membrane-type diamond anvil cell (DAC) equipped with 350 μm culet diamonds. Sodium chloride [20] and ruby [21] were used as pressure calibrants for the $Al_{0.3}Ga_{0.7}PO_4$ and $GaPO_4$ experiments, respectively. In order to have a constant sample thickness for XAS measurements, the gasket holes were filled completely with loosely packed powder to minimize intergranular contacts. A 16:3:1 methanol:ethanol:H_2O pressure-transmitting medium (PTM) was used for the experiment on $Al_{0.3}Ga_{0.7}PO_4$.The amount of water present in the gasket hole did not lead to complete dissolution of the NaCl. The experiment on $GaPO_4$ was performed isothermally at 320 °C without a PTM in order to maximize the XAS signal. The heating of the sample, which also reduces nonhydrostatic stress, was performed using an external resistive heater and the temperature was measured with a thermocouple, which was placed in contact with the diamond anvil. The diamond anvil cells were oriented in the beam to minimize glitches in the XAS spectra due to diffraction from the diamonds. ID24, which is an energy-dispersive x-ray absorption spectrometer, offers the advantage of visualizing the spectrum over the whole energy range in "live" mode and therefore, in a reasonably short time, the glitches can be removed from the energy region of interest by following their energy position as a function of the diamond's orientation. EXAFS signals were analyzed using the Athena software for signal extraction (IFEFFIT) and Artemis for fitting the EXAFS spectra [22]. Full profile fitting of the x-ray diffraction data using the Le Bail method was performed with the program FullProf [23].

C. High-pressure Raman measurements

Raman measurements on $Al_{0.7}Ga_{0.3}PO_4$, $Al_{0.3}Ga_{0.7}PO_4$, and $GaPO_4$ were performed with the Jobin-Yvon T64000 confocal micro-Raman spectrometer in both simple (notch filter) and triple-monochromator configurations using a 50× microscope objective. The 514.532 nm line from a Coherent argon ion laser was used for excitation. The experiments at high pressure were performed with an Easylab Helios membrane diamond anvil cell. The holes of between 100 and 120 μm in diameter in the 70 μm thick preindented stainless steel gaskets were filled with the powdered samples, ruby spheres, and 16:3:1 methanol:ethanol:H_2O as a PTM. The pressure in the DAC was determined from the spectral shift of the ruby R_1 fluorescence line [21]. The recovered sample was also remeasured at room conditions.

D. Theoretical methodology: Evolutionary algorithm procedures and first-principles calculations

In order to identify the stable ground-state structures and compositions in the $GaPO_4$ system, we have employed the first-principles evolutionary structure prediction method USPEX [24–26]. USPEX searches for the global minimum of free energy of the crystal with respect to its structural parameters. As no assumptions are made regarding the structure or its symmetry, this algorithm is capable of discovering completely unexpected or even hitherto unknown crystal structure types [27]. At a given pressure ($P = 5$ and 20 GPa), a fixed stoichiometry crystal structure search is performed using up to 4 formula units per primitive unit cell. The first generation had 80 randomly produced candidate structures; all subsequent generations contained 60 structures. Evolutionary variation operators were applied to search for the global energy minimum; 50% of the new structures were produced by heredity, with the remaining structures were produced by atomic mutation (10%), lattice mutation (10%), permutation (10%), and random generator (20%).

Density functional total energy calculations and geometry optimizations were performed using the VASP program [27] with the Perdew-Burke-Ernzerhof parametrization of the generalized gradient approximation [28] (GGA/PBE). We used projector-augmented wave (PAW) [29] potentials for Ga (Ga_d), P, and O with radii 2.3 a.u. for Ga ([Ar] core), 1.9 a.u. for P ([Ne] core), and 1.52 a.u. for O ([He] core). A plane-wave basis set with a kinetic energy cutoff of 520 eV was employed. We used uniform Γ-centered meshes with a reciprocal space resolution of $2\pi \times 0.06\,\text{Å}^{-1}$ for Brillouin zone sampling to ensure the error bars of the total energies were less than 1 meV/atom. Structure relaxations proceeded until all forces on atoms were less than 1 meV/Å and the total stress tensor had deviations from target pressure within 0.01 GPa.

Images of crystal structures and electronic isosurface maps were produced by VESTA [30].

The Raman spectrum of the candidate orthorhombic $Pmn2_1$ structure for the high-pressure phase of $GaPO_4$ at 20 GPa was calculated at the GGA/PBE level. This calculation was performed using the ABINIT package [31] according to the procedure described in [32]. Dynamical matrix and linear optical susceptibility were obtained within a variational approach to density functional perturbation theory. Derivatives of the linear optical susceptibility with respect to atomic displacements were calculated from finite differences using a displacement of 0.01 bohrs. Convergence was reached for a 60 Ha plane-wave kinetic energy cutoff and a 8 × 8 × 8 mesh of special *k* points.

III. RESULTS AND DISCUSSION

A. Compression of the α-berlinite-type phase and high-pressure phase transition

1. X-ray diffraction

Structural data at both short range (XANES+EXAFS) and long range (x-ray diffraction) were obtained as a function of *P* and *T* for $Al_{0.3}Ga_{0.7}PO_4$ and $GaPO_4$. $Al_{0.3}Ga_{0.7}PO_4$ was compressed at ambient temperature and then heated to 340 °C at 25 GPa. The initial compression behavior of the

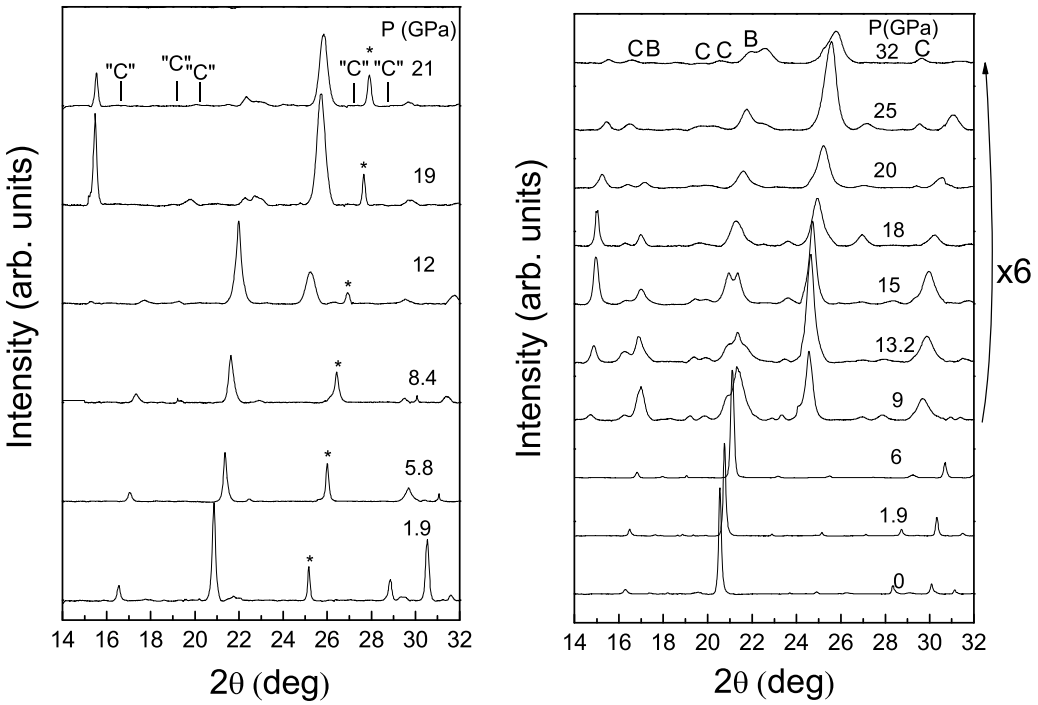

FIG. 1. X-ray diffraction patterns of $Al_{0.3}Ga_{0.7}PO_4$ at 25 °C (left) and $GaPO_4$ at 320 °C (right) as a function of pressure on compression. (* = NaCl pressure calibrant, B = remaining berlinite-type $GaPO_4$, C = $CrVO_4$-type $GaPO_4$, "C" = expected positions for $CrVO_4$-type $Al_{0.3}Ga_{0.7}PO_4$).

α-berlinite-type phase was in good agreement with previous work [17]. Beginning at between 9 and 12 GPa, new diffraction features were observed (Fig. 1). A new crystalline phase was obtained, which was characterized by broad diffraction lines with a highly inhomogeneous intensity distribution in the 2D diffraction images indicating poor crystallinity and strong preferred orientation effects (see Supplemental Material (SM) [33], Fig. S1). This renders structural determination difficult. The most prominent diffraction lines of this phase lie at 4.447, 2.684, and 2.338 Å (15.51°, 25.84°, and 29.71° in 2θ, respectively) at 21 GPa and are distinct from those expected for an orthorhombic $CrVO_4$-type structure. However, above 20 GPa, some very weak diffraction lines at positions where those of an orthorhombic $CrVO_4$-type form could be expected were observed. This phase remained at an impurity level with respect to the new unidentified phase even after heating to 340 °C at 25 GPa. Upon pressure release, the sample retransformed to the α-berlinite-type phase.

In order to determine the effect of temperature on the competition between these two structures $GaPO_4$ was studied isothermally at 320 °C up to 32 GPa. New diffraction features appeared beginning near 9 GPa, which is slightly lower than in previous ambient-temperature studies. Again the data exhibited poor crystallinity and strong preferred orientation (Fig. S1 of the SM). However, in contrast to $Al_{0.3}Ga_{0.7}PO_4$, strong diffraction features corresponding to the orthorhombic $CrVO_4$-type form were observed in addition to the principal lines of the new unidentified phase observed for the solid solution [d = 4.467, 2.692, and 2.346 Å (15.44°, 25.75°, and 29.60° in 2θ, respectively) for $GaPO_4$ at 32 GPa and 320 °C]. The unit cell of the $CrVO_4$-type form at 32 GPa and 320 °C was refined and the following values obtained: space group $Cmcm$, $a = 5.157(17)$ Å, $b = 7.030(14)$ Å, $c = 5.680(12)$. This is consistent with previous measurements on this phase [8,9,34]. The pressure was decreased to 15 GPa at 320 °C and then final decompression was performed at ambient temperature. On pressure release, a mixture of the berlinite-type and these two high-pressure phases was retained.

2. XAS spectroscopy

The XAS spectra of $Al_{0.3}Ga_{0.7}PO_4$ and $GaPO_4$ (Fig. 2 and Fig. S2 of the SM) obtained at ambient pressure are in good agreement with spectra of α-berlinite-type $GaPO_4$ reported in the literature [35]. Changes in the XANES region of the spectra are observed at 12 and 10 GPa respectively for $Al_{0.3}Ga_{0.7}PO_4$ and $GaPO_4$ in agreement with the x-ray diffraction data. At high pressure, the spectra (Fig. 2) bear some resemblance to those of α-Ga_2O_3, in which Ga is in sixfold coordination, thereby providing evidence for an increase in the coordination number of gallium from 4 to 6 as has been reported previously [12]. More quantitative information confirming this increase in coordination number can be obtained by analysis of the EXAFS data. Details of the data analysis along with examples at selected pressures are given in the Supplemental Material [33] (Figs. S3–S7). As expected, the Ga-O bond distance in $GaPO_4$ (Fig. 3) undergoes initial compression prior to the phase transition. Fitting the data for $GaPO_4$ above the phase transition at 11.4 GPa was possible taking into account two contributions corresponding to 4 oxygen atoms at 1.759 Å and 6 at 1.883 Å in a 45:55 ratio. The ratio was calculated based on the amplitudes arising from the two different coordination environments normalized by the number of atoms in the first shell. The corresponding fit at 30 GPa gives 4 oxygen atoms

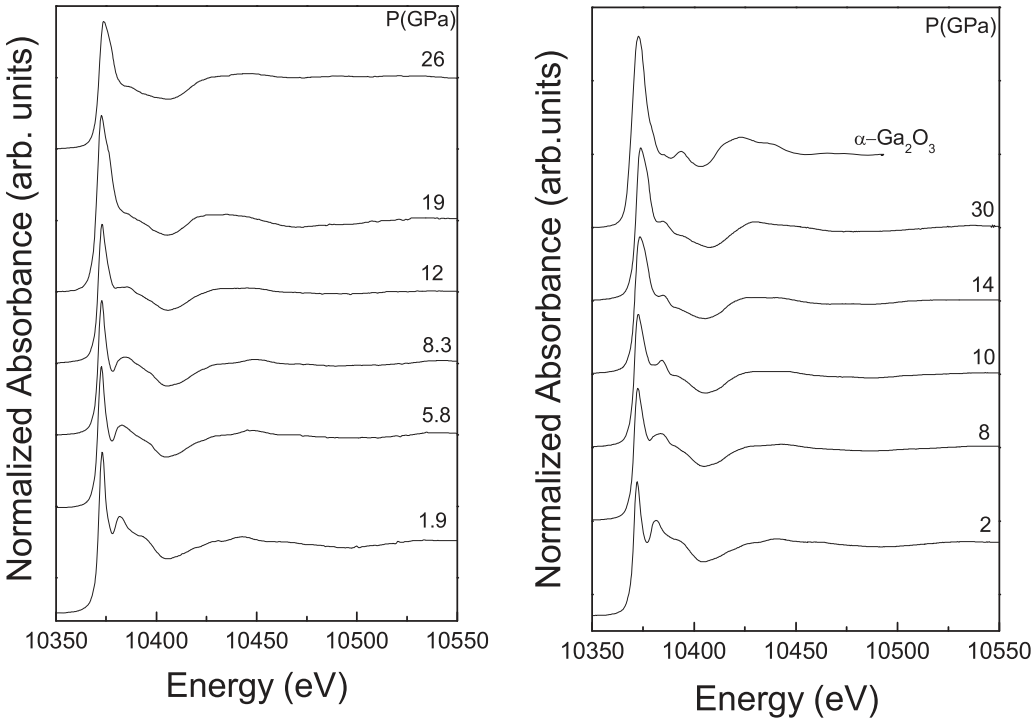

FIG. 2. X-ray absorption spectra of $Al_{0.3}Ga_{0.7}PO_4$ (left) and $GaPO_4$ (right) as a function of pressure on compression. (The ambient-pressure α-Ga_2O_3 data are from [35].)

at 1.73 Å and 6 at 1.866 Å in a 30:70 ratio. Based on the diffraction data, the contribution corresponding to fourfold coordination can be assigned to remaining α-berlinite-type material, whereas the sixfold coordination contribution is due to the high-pressure phases. The increase in Ga-O bond length, Fig. 3, by about 7% due to the increase in coordination number of gallium from 4 to 6 is consistent with previous work on $GaAsO_4$ at high pressure [5,12].

3. *Raman spectroscopy*

Group theory predicts that the pure end member α-berlinite-type $GaPO_4$ (trigonal $P3_121$ D_3^4, $Z = 3$) will exhibit 54 modes of vibration:

$$\Gamma = 8A_1 + 10A_2 + 18E.$$

One A_2 and one 1 E mode are acoustic and the remaining optical modes are

$$\Gamma = 8A_1 + 9A_2 + 17E.$$

There are 25 distinct modes that are predicted to be Raman active (8 nondegenerate $A_1 + 17$ doubly degenerate E). The situation is more complicated for the $Al_{1-x}Ga_xPO_4$ solid solutions. Certain modes involving Al and/or Ga have been found to be coupled leading to one mode [16], which varies continuously in frequency as a function of composition between the two end members due to the difference in mass between Al and Ga. Other modes linked to either AlO_4 or GaO_4 tetrahedra are decoupled [16] such as the librational modes of the AlO_4 or GaO_4 tetrahedra at 229 and 296 cm^{-1}, Table I, which exhibit strong temperature dependence [16,41,42] and in the case of $AlPO_4$ have been linked to soft-mode or incipient soft-mode behavior [41].

The pressure-induced shifts in wave number of the modes of the α-berlinite-type phases of the three compositions studied, Table I, Figs. 4 and 5, are very similar and are in good agreement with previous studies on α-berlinite-type $GaPO_4$ [13,42]. Beginning at pressures of 13 GPa for $x = 0.3$ and 12 GPa for $x = 0.7$ and $x = 1$, very important spectral changes are observed (Figs. 4 and 5) with the gradual disappearance of the vibrational modes of the α-berlinite-type phase and the appearance of a series of new modes, Table II. The principal new modes lie in the 340–460 cm^{-1} and in the 550–630 cm^{-1} regions. The spectra are distinct from the known spectrum of $CrVO_4$-type $GaPO_4$ [9,43], which is obtained essentially in a pure form upon compression of α-cristobalite-type $GaPO_4$. The spectrum of $CrVO_4$-type $GaPO_4$ is relatively simple, with at 17 GPa [43] the strongest peak appearing at 574 cm^{-1} and the second important peak at 314 cm^{-1}. The spectra obtained in the present study are more complex, indicative of a larger unit cell and/or a lower-symmetry structure. It cannot be excluded for $x = 1$ that the $CrVO_4$-type peaks may also be present, but they are weaker than the peaks from the new metastable, high-pressure phase. Above 14 GPa, the remaining peaks of the initial α-quartz-type phase are weak indicating a high degree of conversion to the high-pressure forms. As in the case of $CrVO_4$-type $GaPO_4$ [9], the presence of peaks at close to 550–630 cm^{-1} can be taken as evidence for aluminium and gallium in sixfold coordination. In the spectrum of α-berlinite-type $GaPO_4$ at ambient pressure, the Ga-O stretching vibrations are very weak and are observed in the 600–700 cm^{-1} region [16]. These modes are observed in the 650–750 cm^{-1} region at 11 GPa. In contrast, the P-O

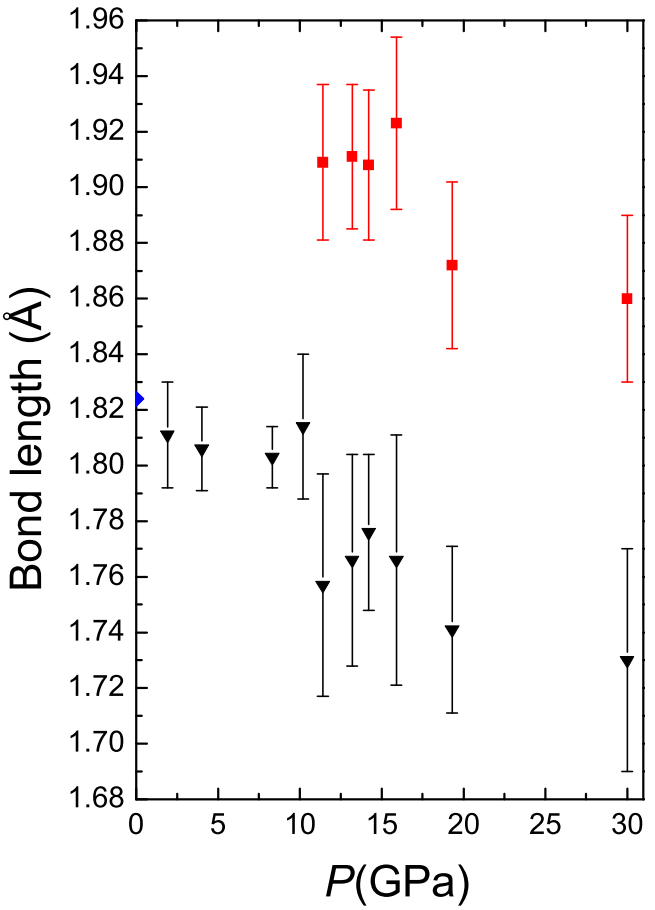

FIG. 3. Ga-O bond length in $GaPO_4$ as a function of pressure at 320 °C on compression. (The ambient-pressure value is from total neutron scattering at high temperature [36].)

stretching modes are observed above 1000 cm^{-1} in the new phase providing evidence for the existence of PO_4 tetrahedra. A significant hysteresis is observed for the transition with retransformation to the initial phase occurring below 10 GPa for $x = 0.3$ and below 8 GPa for $x = 0.7$ and $x = 1$.

4. First-principles evolutionary crystal structure prediction

We used the evolutionary algorithm USPEX to investigate candidates for high-pressure (meta)stable structures of gallium orthophosphate ($GaPO_4$). We performed fully unconstrained variable-cell USPEX simulations at 5 and 20 GPa, using no experimental information such as lattice parameters, space group symmetry, etc. Among the predicted structures at 5 and 20 GPa, the structures with the lowest enthalpies are used to investigate their relative stability as a function of pressure (see Fig. 6). Lattice constants and structural parameters of the most interesting candidate structures are given in the Supplemental Material [33], Table S1. Note that the calculated lattice constant of the $CrVO_4$-type $Cmcm$ phase at 32 GPa ($T =$ 0 K) is in excellent agreement with the experimental value ($T = 593$ K), which gives a benchmark of the typical accuracy to expect of density functional theory (DFT) simulations for this system.

Our theoretical study indicates that the $CrVO_4$-type form of $GaPO_4$ (space group $Cmcm$) has the lowest enthalpy ($G = H$ at $T = 0$ K) from roughly 5 to at least 20 GPa. At 5 GPa, we note a tiny enthalpy difference between orthorhombic $Cmcm$ and α-berlinite-type $P3_121$ phases. Our calculated phase transition pressure from $P3_121$ to $Cmcm$ is 4.7 GPa at $T = 0$ K, but one has to be reminded that the possibility of a large kinetic barrier for the α-berlinite-type $P3_121$ phase to $Cmcm$ phase transformation has to be considered. Even if the $Cmcm$ phase is calculated to be ground state at 5 GPa, higher pressure and/or thermal activation may be needed to reach it. As shown in Fig. 6, the α-berlinite-type phase $P3_121$ becomes thermodynamically unstable relative to all proposed low-enthalpy structures when external pressure is higher than roughly 12 GPa. Recall that the $P3_121$ phase contains fourfold-coordinated Ga atoms (GaO_4 units) while the other predicted structures possess octahedral GaO_6 units. The PO_4 tetrahedra remain unaltered from 4 to 20 GPa, in agreement with the well-known rigidity of these PO_4 units. As we are looking for metastable phases at high pressure, we focus our attention at the low-enthalpy structures located on the potential energy surface of $GaPO_4$ at 20 GPa. At 20 GPa, the second lowest structure is $P1$, located at +9 meV/atom (+20 meV/atom at 10 GPa) from $Cmcm$. This phase becomes lower in energy than $Cmcm$ above 30 GPa. This $P1$ structure consists of stacked infinite chains of edge-sharing distorted GaO_6 octahedra and the linkage between GaO_6-based chains is made by PO_4 tetrahedra (see Fig. S8 in the SM). At 20 GPa, four other low-enthalpy structures are located in the energy range from +32 to +43 meV/atom to the ground state $Cmcm$, namely $Pmn2_1$, $C2/m$, $Imma$, and $C2$ structures (see Fig. S8 in the SM for detailed crystal structures). As previously mentioned, all of them contain sixfold-coordinated gallium and fourfold phosphorus atoms. These structures mainly differ by the connectivity of the GaO_6 octahedral building units (see Fig. 7). $Cmcm$, $C2/m$, and $Imma$ structures are built up of chains of edge-sharing GaO_6 octahedra. $P1$ and $C2$ Ga-O networks contain linked pairs of edge-sharing GaO_6 octahedra which form infinite chains. Finally, layers of corner-sharing GaO_6 octahedra are present in $Pmn2_1$ structure.

Our evolutionary crystal structure searches lead to four competitive metastable structures for $GaPO_4$ at 20 GPa. In the next section, we will turn our discussion to the comparison of theoretical x-ray diffraction patterns obtained from our *in silico* high-pressure metastable crystal structures with experimental XRD results.

B. Nature of the metastable high-pressure phase

In addition to the stable $CrVO_4$-type phase, which was already identified by x-ray diffraction, the five higher enthalpy structures built up from GaO_6 octahedra and PO_4 tetrahedra obtained in the USPEX search at 20 GPa were considered as potential candidates for the new metastable phase of $GaPO_4$. The diffraction patterns of all these structures were calculated. Only one structure gave rise to a diffraction pattern that bore any similarity to the experimental data (Fig. 8). This was the orthorhombic $Pmn2_1$ structure with calculated lattice parameters of $a = 5.479$ Å, $b = 4.529$ Å, and $c = 4.408$ Å at 20 GPa. Using this structural model, the experimental data

TABLE I. Raman modes (cm^{-1}) and their pressure coefficients (cm^{-1} GPa^{-1}) for α-berlinite-type $Al_{1-x}Ga_xPO_4$ (vw = very weak).

	$x = 0.3$		$x = 0.7$		$x = 1$	
Mode [Refs. [16,37–40]]	$\tilde{v}$	$d\tilde{v}/dP$	$\tilde{v}$	$d\tilde{v}/dP$	$\tilde{v}$	$d\tilde{v}/dP$
E	1222		1206		1195	
E, A_1	1096	-1.3 ± 0.3	1081	-0.9 ± 0.4	1070	-1.8 ± 0.2
A_1	1075		1066		1061	
E	vw		741			
A_1	vw		714	3.0 ± 0.8		
E	vw		672	3.9 ± 0.3	676	
A_1	vw		vw		661	
E	vw		vw			
E	vw		610	3.8 ± 0.2	603	
E, A_1	462	5.8 ± 0.2	461	5.9 ± 0.2	459	5.9 ± 0.3
E, A_1	437	2.91 ± 0.1	433	3.0 ± 0.8	431	2.8 ± 0.2
E	421		412		414	
E, A_1	300	5.42 ± 0.3	296	5.5 ± 0.5	296	5.7 ± 0.77
A_1	229		229			
A_1	199		191		185	
E	Vw		vw		191	
E, A_1	156	-0.14	150	-0.5 ± 0.1	146	-0.4
E	120	1.6 ± 0.2	118	2.3 ± 0.2	116	2.3 ± 0.1
E	107		105		101	

could be readily indexed and the unit cell refined giving $a = 5.507(13)$ Å, $b = 4.487(19)$ Å, and $c = 4.268(21)$ Å at 32 GPa and 320 °C. The $CrVO_4$ and some of the initial berlinite-type form were present as secondary phases. The unit cell volume is 105.5(7) $Å^3$, which indicated that this structure is about 3% less dense than the stable $CrVO_4$ form under the same *P-T* conditions. The data obtained for the $Al_{0.3}Ga_{0.7}PO_4$ solid solution at 21 GPa could also be indexed with this model. As the data are of relatively better quality for this material, in particular due to the higher purity of this phase with only some remaining berlinite-type form as the principal secondary phase, it was possible to perform a fit by the Le Bail method (Fig. 9) to obtain the unit cell parameters giving $a = 5.52(6)$ Å, $b = 4.446(3)$ Å, $c = 4.27(3)$ Å. These results indicate that this $Pmn2_1$ structure is a very reasonable model for this new metastable phase for which the diffraction data are of modest quality due to the presence of secondary phases, preferred orientation, and line broadening (Fig. S1 of the SM).

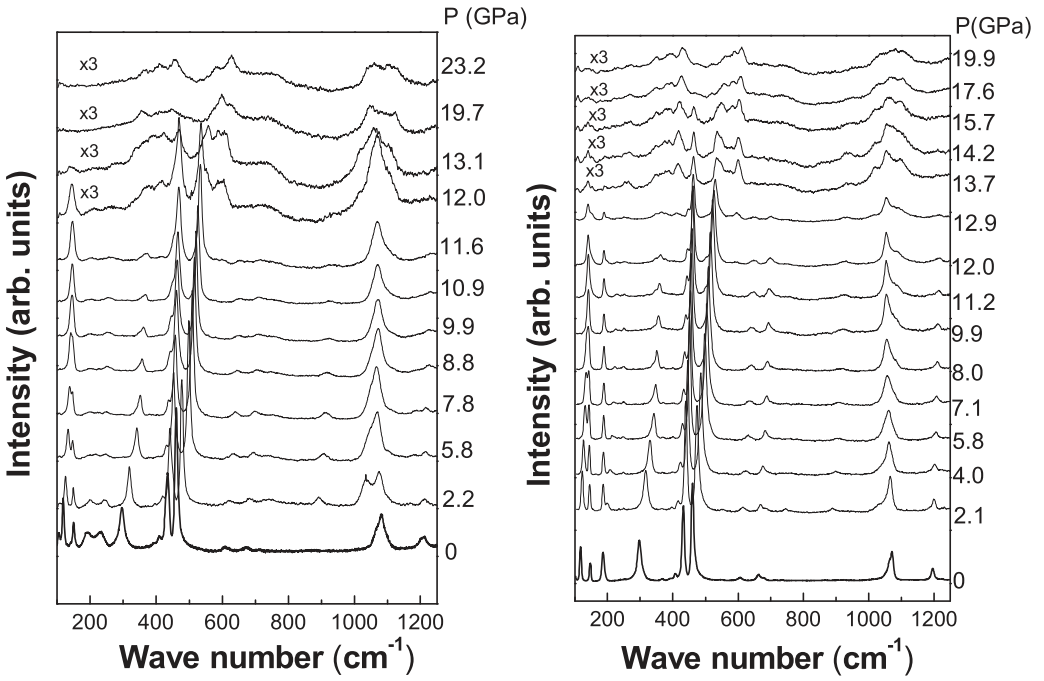

FIG. 4. Raman spectra of $Al_{0.3}Ga_{0.7}PO_4$ (left) and $GaPO_4$ (right) as a function of pressure.

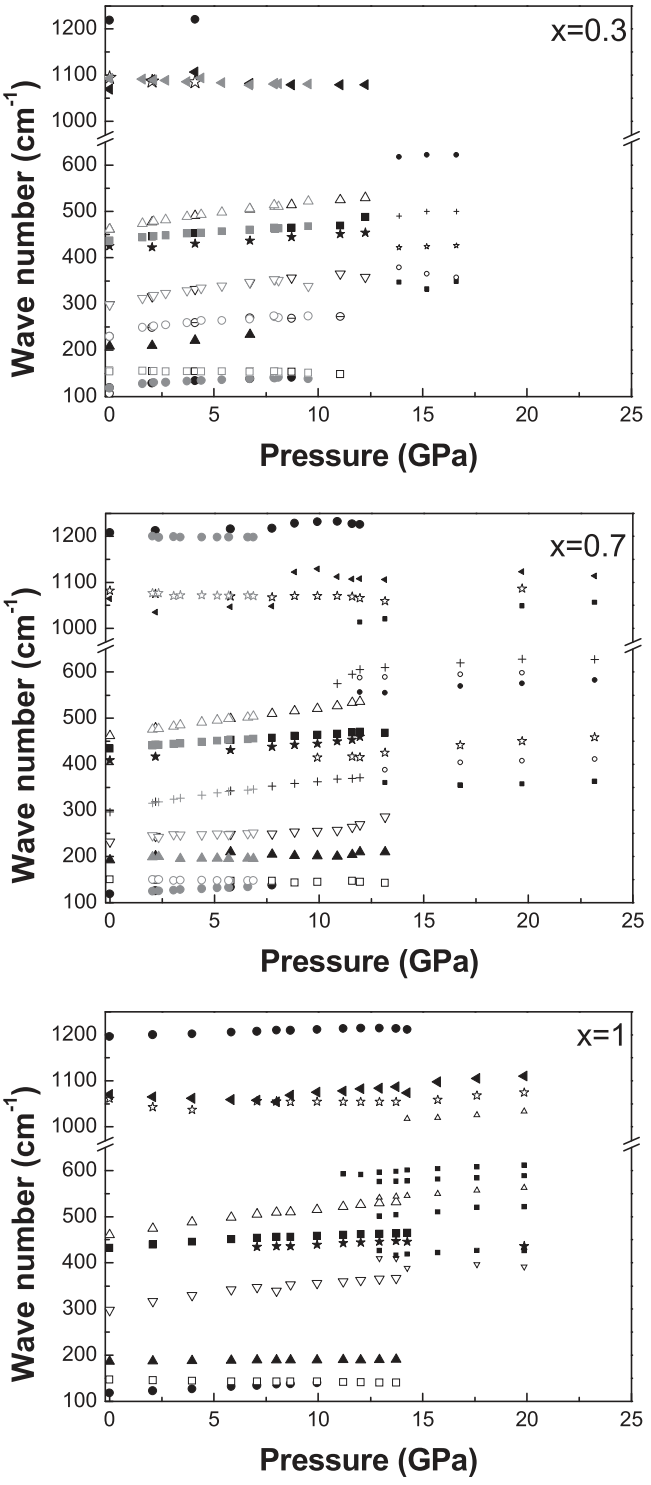

FIG. 5. Pressure dependence of the Raman modes of $Al_{1-x}Ga_xPO_4$ as a function of pressure.

In order to further test this hypothesis, the Raman spectrum of this phase was calculated by DFT (Fig. 10 and Table III). The obtained spectrum can be compared to the experimental data, which are characterized by a relatively weak signal. The difference between the calculated and experimental Raman shifts varies between 0 and 6%, which is very similar to the differences observed for the starting berlinite-type phase [44]

TABLE II. Principal Raman modes (cm^{-1}) and their pressure coefficients ($cm^{-1}\,GPa^{-1}$) for the high-pressure form(s) of $Al_{1-x}Ga_xPO_4$. The remaining modes from the α-berlinite-type phase are not included in the table.

$x = 0.3$, 16.6 GPa		$x = 0.7$, 23.2 GPa		$x = 1$, 19.9 GPa	
$\tilde{\nu}$	$d\tilde{\nu}/dP$	$\tilde{\nu}$	$d\tilde{\nu}/dP$	$\tilde{\nu}$	$d\tilde{\nu}/dP$
		1114	4 ± 0.5	1110	
1067				1074	
1032		1056	3.9 ± 0.1	1034	3.1 ± 0.2
622	1.5 ± 1	627	1.9 ± 0.2	612	1.6 ± 0.3
		595	2.6 ± 0.1	589	2 ± 0.2
		583	1.2 ± 0.1	563	2.8 ± 0.4
426	1.5 ± 0.1	459	3.4 ± 0.4	432	1.6 ± 0.3
		411	2.3 ± 0.1	392	
357		363	0.7 ± 0.3	349	0.7 ± 0.2

using the same method of calculation. As for the starting phase, the origin of the difference between the calculated and experimental Raman spectra could arise from the approximations involved in the calculation (mainly the choice of the exchange-correlation functional and the harmonic approximation used to build the dynamical matrix) combined with the methodology used for modeling a powder from calculations on a single crystal. Nevertheless, the observed differences in Raman shift and intensity remain satisfactory considering this type of calculation and approach. In addition, no soft modes are calculated at the Γ point. Although the present results cannot definitely be used to determine the structure of this phase, the $Pmn2_1$ structure is by far the best model available.

The $Pmn2_1$ structure is built up of layers of corner-sharing GaO_6 octahedra in the yz plane linked by PO_4 tetrahedra with one shared edge between tetrahedra and octahedra in the **a** direction. This is very different from the $Cmcm$ structure, which is built up of chains of edge-sharing GaO_6 octahedra in the **c** direction linked by corner sharing by PO_4 tetrahedra in

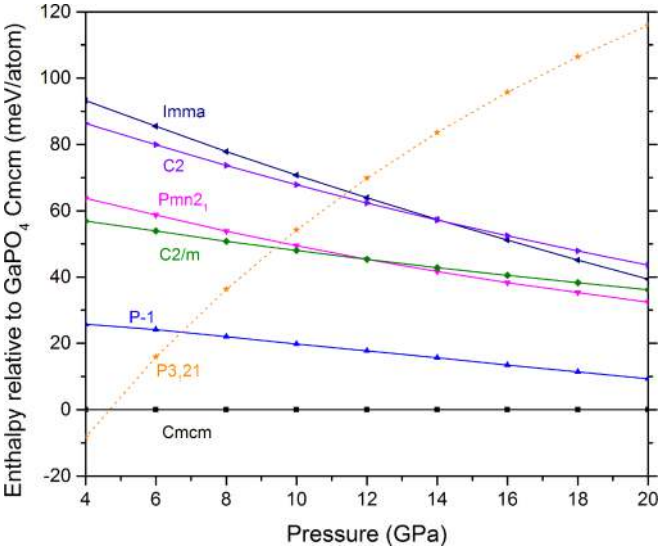

FIG. 6. Static ground-state enthalpies (per atom) of various $GaPO_4$ structures relative to the $CrVO_4$-type $Cmcm$ phase as a function of pressure. Structures contain four-coordinated (dashed line) or six-coordinated Ga atoms (solid lines).

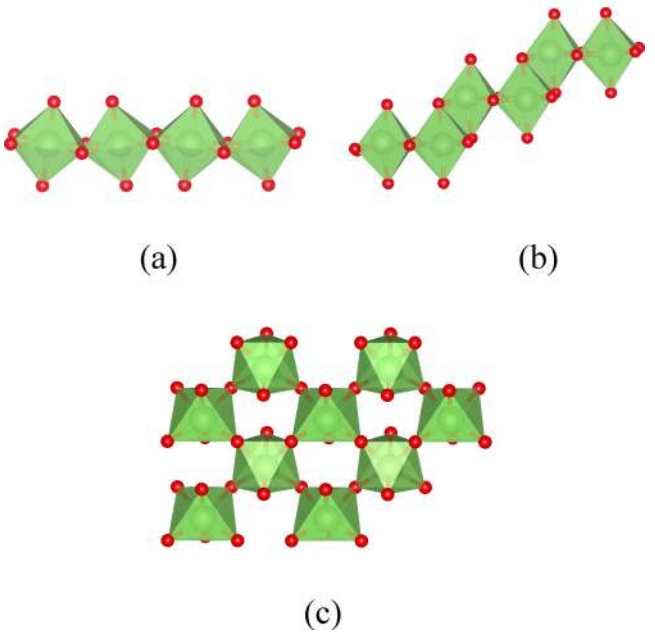

FIG. 7. GaO_6-based motifs encountered in computed low-enthalpy structures of $GaPO_4$ at 20 GPa. (a) Edge-sharing, (b) linked pairs of edge-sharing, and (c) layer of corner-sharing GaO_6 octahedra.

the other directions. It can be noted that in the low-pressure α-berlinite-type structure all tetrahedra share corners.

The stable high-pressure phase with the $CrVO_4$ structure is obtained on heating at high pressure from berlinite-type $GaPO_4$ [8]. In contrast, α-cristobalite $GaPO_4$, which is based on a cubic close-packed oxygen sublattice, can transform to the $CrVO_4$ phase at ambient temperature [9,34] via a displacive mechanism [45]. The present results show that starting from

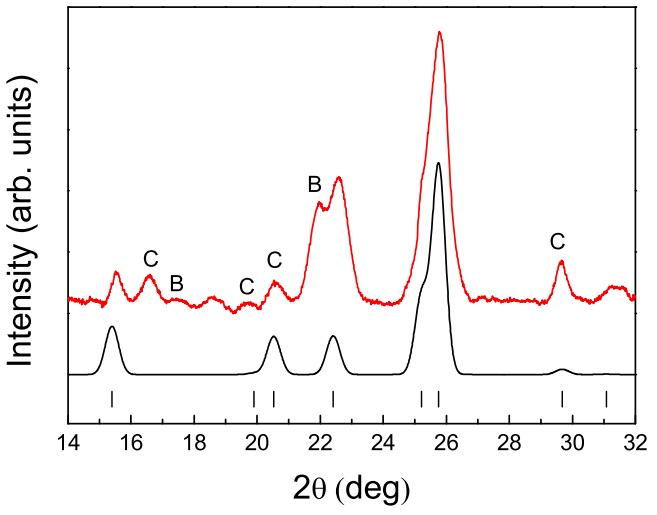

FIG. 8. Experimental (upper graph) x-ray diffraction pattern of $GaPO_4$ at 32 GPa and 320 °C and calculated pattern (lower graph) using the refined experimental unit cell parameters and the fractional atomic coordinates of the $Pmn2_1$ structure from first-principles calculations. Vertical bars indicate the refined positions of the Bragg reflections for the $Pmn2_1$ structure. (B = remaining berlinite-type $GaPO_4$, C = $CrVO_4$-type $GaPO_4$).

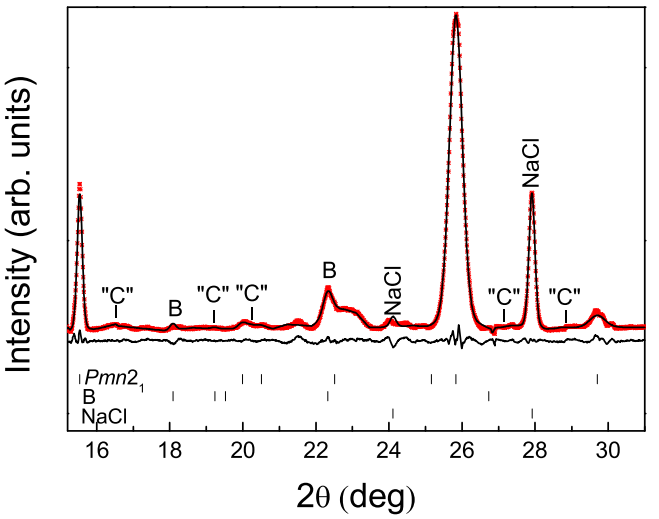

FIG. 9. Experimental x-ray diffraction pattern (red symbols) of $Al_{0.3}Ga_{0.7}PO_4$ at 21 GPa and 25 °C and calculated and difference patterns from a Le Bail fit (solid lines) with the following refined experimental unit cell parameters for the $Pmn2_1$ structure: a = 5.52(6) Å, b = 4.446(3) Å, c = 4.27(3) Å (agreement factors r_p = 8.6%, r_{wp} = 4.0%). Vertical bars indicate the refined positions of the Bragg reflections. (NaCl = NaCl pressure calibrant, B = remaining berlinite-type $GaPO_4$, C = $CrVO_4$-type $GaPO_4$, "C" = expected positions for $CrVO_4$-type $Al_{0.3}Ga_{0.7}PO_4$.)

the berlinite-type phase, a new orthorhombic $Pmn2_1$ structure is obtained at high pressure and ambient temperature or with moderate heating. This transition can be expected to

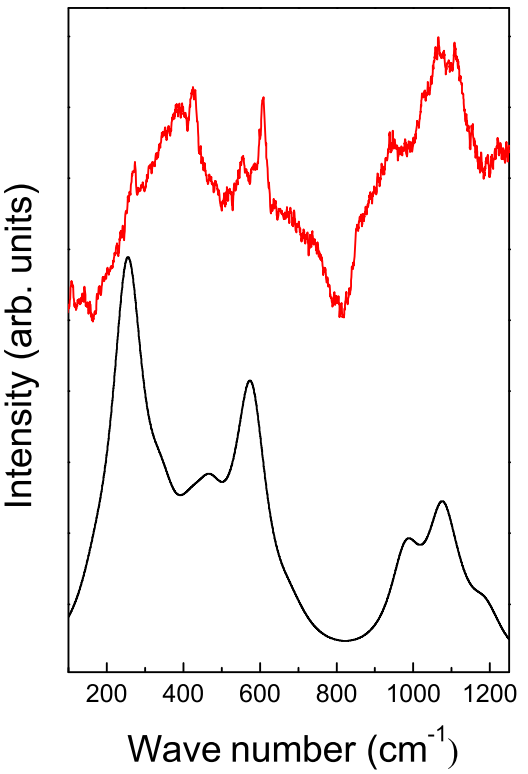

FIG. 10. Experimental (upper) Raman spectrum of $GaPO_4$ at 19 GPa on decompression and the spectrum from DFT using the $Pmn2_1$ structure (lower). The calculated FWHM is arbitrary.

TABLE III. Calculated Raman modes (cm^{-1}) for $Pmn2_1$-type $GaPO_4$ and experimental data at 19 GPa on decompression.

Mode	$\tilde{v}$ (calc)	$\tilde{v}$ (expt)
B_2	1212	1224
A_1	1187	1153
B_2	1116	1107
A_1	1076	1065
A_1	981	1028
B_2	980	
A_2	972	
B_1	909	946
B_2	711	
A_1	677	
A_1	576	607
A_2	575	
B_2	571	
B_1	559	587
B_2	527	555
A_2	489	
B_1	488	
A_1	468	468
A_1	426	422
B_1	410	390
B_2	403	
A_2	354	
B_1	348	351
A_2	337	
B_2	322	
A_1	279	
B_2	275	
A_1	254	269
A_2	247	
B_1	211	
B_2	187	
A_2	172	
A_1	167	

be less reconstructive than the berlinite-$CrVO_4$ transition. This is similar to what occurs in α-quartz, where at ambient temperature transitions occur to metastable monoclinic $P2_1/c$ and $P2/c$ phases [2,46] via diffusionless pathways [47]. As the phase is metastable, its presence in a given experiment will depend on time (transition kinetics), temperature (in the absence of enough thermal activation to obtain the stable high-pressure form), and nonhydrostatic stress, which could favor certain energetic pathways.

IV. CONCLUSIONS

A combination of experiment and first-principles calculations was used to investigate the high-pressure phase transitions in $GaPO_4$ and the $AlPO_4$-$GaPO_4$ solid solution. X-ray absorption and Raman spectroscopy are consistent with an increase in the coordination number of Ga to 6 with the phosphorus remaining in 4-fold coordination. Raman spectroscopy and x-ray diffraction provide evidence for a new metastable high-pressure phase in addition to the stable $CrVO_4$-type form. In the case of the solid solution, the sample consisted essentially of the new metastable phase, indicating that cation disorder or the smaller cation size of aluminum are favorable factors for its metastability. First-principles calculations and the evolutionary algorithm USPEX were used to predict possible high-pressure structures in this system. The experimental data were consistent with one predicted metastable orthorhombic structure, space group $Pmn2_1$. This structure is found to be present at ambient temperature and after heating at moderate temperatures up to 320–340 °C indicating the presence of a non-negligible activation energy for a reconstructive phase transition to the stable $CrVO_4$-type form. This can be understood by the major difference between the structures of the $CrVO_4$-type form based on chains of edge-sharing GaO_6 octahedra and the orthorhombic $Pmn2_1$ structure built up of layers of corner-sharing GaO_6 octahedra.

[1] R. J. Hemley, A. P. Jephcoat, H. K. Mao, L. C. Ming, and M. H. Manghnani, Nature (London) **334**, 52 (1988).

[2] J. Haines, J. M. Léger, F. Gorelli, and M. Hanfland, Phys. Rev. Lett. **87**, 155503 (2001).

[3] K. J. Kingma, C. Meade, R. J. Hemley, H. K. Mao, and D. R. Veblen, Science **259**, 666 (1993).

[4] J. Haines and O. Cambon, Z. Kristallogr. **219**, 314 (2004).

[5] A. Polian, J. P. Itié, J. Badro, M. Grimsditch, and E. Philippot, Eur. J. Solid State Inorg. Chem. **34**, 669 (1997).

[6] M. P. Pasternak, G. Kh. Rozenberg, A. P. Milner, M. Amanowicz, T. Zhou, U. Schwarz, K. Syassen, R. D. Taylor, M. Hanfland, and K. Brister, Phys. Rev. Lett. **79**, 4409 (1997).

[7] J. Pellicer-Porres, A. M. Saitta, A. Polian, J. P. Itié, and M. Hanfland, Nat. Mater. **6**, 698 (2007).

[8] J. Badro, J. P. Itié, and A. Polian, Eur. Phys. J. B **1**, 265 (1998).

[9] J. L. Robeson, R. R. Winters, and W. S. Hammack, Phys. Rev. Lett. **73**, 1644 (1994).

[10] Ph. Gillet, J. Badro, B. Varrel, and P. F. McMillan, Phys. Rev. B **51**, 11262 (1995).

[11] S. M. Sharma, N. Garg, and S. K. Sikka, Phys. Rev. B **62**, 8824 (2000).

[12] J. P. Itié, T. Tinoco, A. Polian, G. Demazeau, S. Matar, and E. Philippot, High Press. Res. **14**, 269 (1996).

[13] M. J. Peters, M. Grimsditch, and A. Polian, Solid State. Commun. **114**, 335 (2000).

[14] J. Haines, O. Cambon, D. Cachau-Herreillat, G. Fraysse, and F. E. Mallassagne, Solid State Sci. **6**, 995 (2004).

[15] J. Haines, O. Cambon, G. Fraysse, and A. Van der Lee, J. Phys.: Condens. Matter **17**, 4463 (2005).

[16] E. Angot, R. Le Parc, C. Levelut, M. Beaurain, P. Armand, O. Cambon, and J. Haines, J. Phys.: Condens. Matter **18**, 4315 (2006).
[17] J. Haines, O. Cambon, R. Le Parc, and C. Levelut, Phase Trans. **80**, 1039 (2007).
[18] G. Aquilanti, W. Crichton, and S. Pascarelli, High Press. Res. **23**, 301 (2003).
[19] A. P. Hammersley, S. O. Svensson, M. Hanfland, A. N. Fitch, and D. Häusermann, High Pressure Res. **14**, 235 (1996).
[20] F. Birch, J. Geophys. Res. **91**, 4949 (1986).
[21] H. K. Mao, J. Xu, and P. M. Bell, J. Geophys. Res. B **91**, 4673 (1986).
[22] B. Ravel and J. M. Newville, J. Synchrotron Radiat. **12**, 537 (2005).
[23] J. Rodriguez-Carvajal, in *Proceedings of the XVIII Conference on Applied Crystallography*, edited by H. Morawiec and D. Stróz (World Scientific, Singapore, 2001), pp. 30–36.
[24] A. R. Oganov and C. W. Glass, J. Chem. Phys. **124**, 244704 (2006).
[25] A. R. Oganov, A. O. Lyakhov, and M. Valle, Acc. Chem. Res. **44**, 227 (2011).
[26] A. O. Lyakhov, A. R. Oganov, H. T. Stokes, and Q. Zhu, Comput. Phys. Commun. **184**, 1172 (2012).
[27] G. Kresse and J. Furthmüller, Phys. Rev. B **54**, 11169 (1996).
[28] J. P. Perdew, K. Burke, and M. Ernzerhof, Phys. Rev. Lett. **77**, 3865 (1996).
[29] P. E. Blöchl, Phys. Rev. B **50**, 17953 (1994).
[30] K. Momma and F. Izumi, J. Appl. Crystallogr. **41**, 653 (2001).
[31] X. Gonze *et al.*., Comput Phys Commun. **180**, 2582 (2009).
[32] P. Hermet, N. Izard, A. Rahmani, and P. Ghosez, J. Phys. Chem. B **110**, 24869 (2006).
[33] See Supplemental Material at http://link.aps.org/supplemental/10.1103/PhysRevMaterials.1.033607 for supplementary figures S1–S8 and Table S1.
[34] L. C. Ming, Y. Nakamoto, S. Endo, C. H. Chio, and S. K. Sharma, J. Phys.: Condens. Matter **19**, 425202 (2007).
[35] P. Charton and P. Armand, J. Non-Cryst. Solids **333**, 307 (2004).
[36] J. Haines, O. Cambon, N. Prudhomme, G. Fraysse, D. A. Keen, L. C. Chapon, and M. G. Tucker, Phys. Rev. B **73**, 014103 (2006).
[37] I. Gregora, N. Magneron, P. Simon, Y. Luspin, N. Raimboux, and E. Philippot, J. Phys.: Condens. Matter **15**, 4487 (2003).
[38] H. Xia, J. Wang, L. Li, and Z. Zou, Prog. Cryst. Growth Charact. Mater. **40**, 253 (2000).
[39] A. Goullet, J. Pascual, R. Cusco, and J. Camassel, Phys. Rev. B **44**, 9936 (1991).
[40] R. Ouillon, J.-P. Pinan-Lucarre, and P. Ranson, J. Raman Spectrosc. **31**, 605 (2000).
[41] J. F. Scott, Phys. Rev. Lett. **24**1107 (1970).
[42] M. Nakamura, H. Orihara, Y. Ishibashi, P. Kim, and S. Hirano, J. Phys. Soc. Jpn. **59**, 1831 (1990).
[43] C. H Chio, S. K. Sharma, L. C. Ming, Y. Nakamoto, and S. Endo, J. Phys.: Conf. Ser. **121**, 022003 (2008).
[44] M. Souleiman, P. Hermet, A. Haidoux, C. Levelut, J. Haines, and O. Cambon, RSC Adv. **3**, 22078 (2013).
[45] V. V. Murashov, L. S. Dubrovinsky, J. S. Tse, and Y. Lepage, J. Phys.: Condens. Matter **7**, 8279 (1995).
[46] Q. Y. Hu, J. F. Shu, W. G. Wang, C. Park, M. W. Chen, T. Fujita, H. K. Mao, and H. W. Sheng, Phys. Rev. B **95**, 104112 (2017).
[47] D. M. Teter, R. J. Hemley, G. Kresse, and J. Hafner, Phys. Rev. Lett. **80**, 2145 (1998).